Study on Molding Process of UHMWPE Microporous Filter Materials

Qiang Zhang, Mingyin Jia, Ping Xue

Institute of Plastics Machinery and Plastics Engineering, Beijing University of Chemical Technology, Beijing, China, 100029

Received 19 September 2011; accepted 5 January 2012
DOI 10.1002/app.36750
Published online in Wiley Online Library (wileyonlinelibrary.com).

ABSTRACT: A method called loose sintering was first introduced to prepare ultrahigh-molecular weight polyethylene (UHMWPE) microporous materials. The pore size was predicted by the face-centered cubic structure model while considering the particles' arrangement and melt. The results showed that the experimental pore diameter was close to that calculated by the present model. The effects of UHMWPE molecular weight, particle diameter, packing density, sintering temperature, and sintering time on pore size, compressive strength, pore diameter distribution, and density were presented. The morphology of micropore and the uniformity of pore distribution were analyzed by scanning electron microscopy and fractal geometry. The results showed that average pore diameter and porosity both increased with the UHMWPE particle diameter while decreased with compressive strength and bulk density. Sintering temperature and sintering time determined whether the heat was redundant to melt the particles. They also determined the pore size and the uniformity. UHMWPE microporous materials could be successfully prepared with suitable processing conditions. J Appl Polym Sci 000: 000–000, 2012

Key words: UHMWPE; microporous; loose sintering; porosity; pore size

INTRODUCTION

Microporous material is a very important part of filtration and separation technology. As a new type of engineering thermoplastic, ultrahigh-molecular weight polyethylene (UHMWPE) has comprehensive excellent properties of abrasion resistance, self-lubricating property, impact resistance, high-chemical stability, resistance to low temperature, nontoxicity, etc.[1] Hence, UHMWPE has been used to fabricate various products including pipe, panel, bar, shuttle, gear, artificial bone, body armor, and microporous materials. However, UHMWPE has some undesirable properties such as no liquidity, low-critical shearing rate because of its extremely high-molecular weight, which is commercially available in grades ranging from 3.5×10^6 to 6×10^6 kg/mol (ASTM calculation).[2] The undesirable properties make UHMWPE hard to process into microporous materials with traditional methods.

The traditional method for making porous polyethylene bodies is to sinter.[3–5] During the sintering process, polyethylene resin powders are first put into the mold and exerted a certain pressure. Then, the mold is maintained for 3 h at a temperature of 150°C inside a heating cabinet. The surface of polymer particle melts and joins at contact point. The space among particles forms the pore. This method works for UHMWPE to make porous materials. However, such method has low-production efficiency due to its long heating time. Moreover, compressing UHMWPE resin powders during heating could impair the space among particles, which results in low porosity and irregular structure. Thermally induced phase separation (TIPS) proposed by Castro[6] is the common method to prepare UHMWPE microporous materials. According to the process,[7,8] UHMWPE and diluent are blended into a homogeneous phase solution at a high temperature. The diluent used has low-molecular weight and high-boiling point. When it is cooled, homogeneous phase solution undergoes phase separation, and the space from the diluent is the source of pore.[9] Later, TIPS combined with stretching (TIPS-S) was developed by Mrozinski.[10–12] During phase-separation processing, stretching is applied, and it causes the break of amorphous regions between stacked crystalline lamellas aligning to fiber axis. Pore produced by the break of amorphous regions is referred as broken pore. Thereby, TIPS-S can avoid dense surface and obtain high porosity.[13] The minimum pore size is less than 0.01 μm, and the porosity is more than 90% by TIPS-S.[14] Pluyter et al.'s research[15,16] showed that the boiling point of diluent was preferably in 225–250°C, and most preferable diluent was decalin when

Correspondence to: P. Xue (buct_nme@sohu.com).

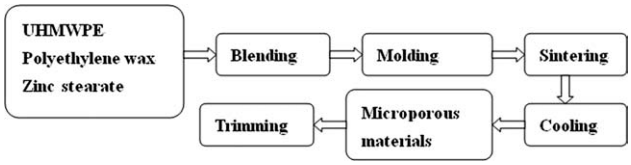

Figure 1 The manufacturing process of UHMWPE microporous materials.

using TIPS-S. Fortuin et al.'s research[17,18] also showed that UHMWPE with molecular weight of beyond 4×10^5 kg/mol at least or even beyond 1×10^6 kg/mol could be used to make microporous materials with sufficient strength and high porosity. However, because diluent could be more homogeneously distributed and more easily extracted in the shape of membrane, TIPS and TIPS-S are just limited to prepare membranes or sheets. Besides, pore size produced by such two methods is usually small ranging from 0.01 μm to a dozen microns, which also limits microporous materials' application. In 2009, Plumlee and Schwartz[19] used inorganic particles as the pore-forming agent to prepare UHMWPE microporous materials. In this process, NaCl is chosen as porogen to blend into UHMWPE resin, and then the product is soaked in a solvent that dissolves away the porogen while leaving voids within the polymer system. Thus, pore diameter strongly depends on the inorganic particle diameter. However, the method has low-production efficiency due to its long processing cycle. Furthermore, thickness of the product is usually small. In 2010, another method adding SiO_2 was used to fabricate UHMWPE/SiO_2 hybrid membrane by Li.[20,21] According to the method, silicon dioxide is blended into UHMWPE as skeleton to improve the microporous materials' pressure resistance, and the maximum pore size is more than 100 μm. However, this method can only produce microporous materials with same section and small thickness.

In this study, a method called loose sintering was proposed to prepare UHMWPE microporous materials, and its pore forming mechanism and pore size model were first proposed. In the model, packing UHMWPE particles was assumed to be arranged as face-centered cubic structure. The surface of UHMWPE particles began to melt and joined together at contact surface when the molding temperature rose to melting temperature. The space remaining among the particles after cooling was the reason of pore forming. In the method, UHMWPE was directly putt into the mold for sintering without pressure, which could effectively avoid low porosity and irregular structure. Moreover, sintering time could sharply reduce to 15 min, and thickness of porous materials was not restricted. The effects of UHMWPE molecular weight, particle diameter, packing density, sintering temperature and sintering time on pore size, compressive strength, pore diameter distribution, and bulk density were also discussed. Moreover, fractal geometry first proposed by Mandelbort[22] was also used to investigate the uniformity of pore distribution.

EXPERIMENTAL

Materials

Different grades of UHMWPE (M2, M3, and M4 type) with weight–average molecular weights of 4.2×10^6 g/mol, 5.2×10^6 g/mol, and 6.0×10^6 g/mol, respectively, were purchased from Beijing No. 2 Reagent Plant (Beijing, China). Polyethylene wax as a component of compound lubricant was provided by Nanjing Yangzi Fine Chemical Co. Zinc stearate was supplied by Tsingdao Kelly Source Chemical Co. The mass ratio of UHMWPE, polyethylene wax and zinc stearate was 250 : 5 : 1 by weight.

Preparation of UHMWPE microporous materials

The procedures for preparing UHMWPE microporous materials are shown in Figure 1. First, UHMWPE, polyethylene wax, and zinc stearate were mixed at 23°C (room temperature) for 1 min by a high-speed mixer machine (SHR-50A, Sanxingjiangfan, CHN). The compound lubricant including polyethylene wax and zinc stearate was used to help UHMWPE particles melt and join together. After mixing uniformly, the blend was putted into the mold to sinter by block press. Before sintering, the mold needed to be shocked for a certain time with electricity to compact polymer particles. The blend was heated to a set temperature (about 200°C) and kept for about 15 min at that temperature without pressure. Then, the hot mold with the blend was

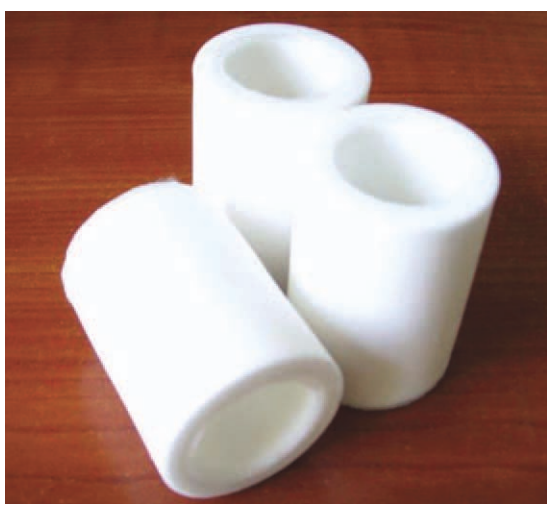

Figure 2 UHMWPE microporous product. [Color figure can be viewed in the online issue, which is available at wileyonlinelibrary.com.]

TABLE I
Experimental Conditions for the Preparation of UHMWPE Microporous Materials

Group	Particle diameter (μm)	Sintering temperature (°C)	Sintering time (min)	Molecular weight (g/mol)
R1	250–355	200	15	4.2×10^6
R2	250–355	200	15	5.2×10^6
R3	250–355	200	15	6.0×10^6
R4	300–355	200	15	4.2×10^6
R5	250–300	200	15	4.2×10^6
R6	150–180	200	15	4.2×10^6
R7	80–106	200	15	4.2×10^6
R8	300–355	210	15	4.2×10^6
R9	300–355	200	25	4.2×10^6

cooled down to room temperature rapidly by intermittent water. Finally, UHMWPE microporous product was prepared and removed from the mold. Figure 2 shows the UHMWPE microporous product prepared by the present method. The experimental conditions for the preparation of different groups of samples are given in Table I. In each group, there are five samples prepared under the same processing conditions.

Physical testing

The compressive strength was measured by universal mechanical testing machine (1185, Instron, UK). The measurement was taken at 23°C with relative humidity of around 45%. The crosshead speed was 5 mm/min. Pore diameter was measured by mercury intrusion porosimeter (AutoPore IV 9500, USA), the extent of intrusion pressure was set from 0.16 to 60,000 psi. Furthermore, pore diameter distribution was studied through the data obtained from mercury intrusion porosimeter. Bulk density and porosity of microporous materials were measured by weight.

SEM observation

The microporous materials were fractured in liquid nitrogen and then sputtered with gold to observe the structure of the cross section by scanning electron microscope (SEM, S-4700, Hitachi, Japan).

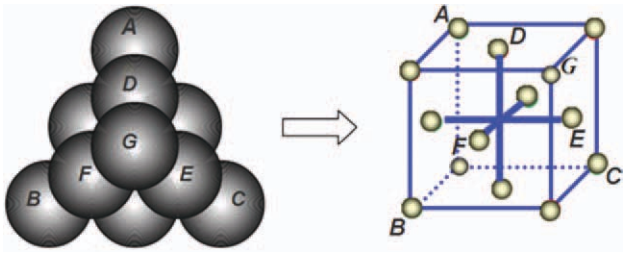

Figure 3 Diagram of face-centered cubic structure model. [Color figure can be viewed in the online issue, which is available at wileyonlinelibrary.com.]

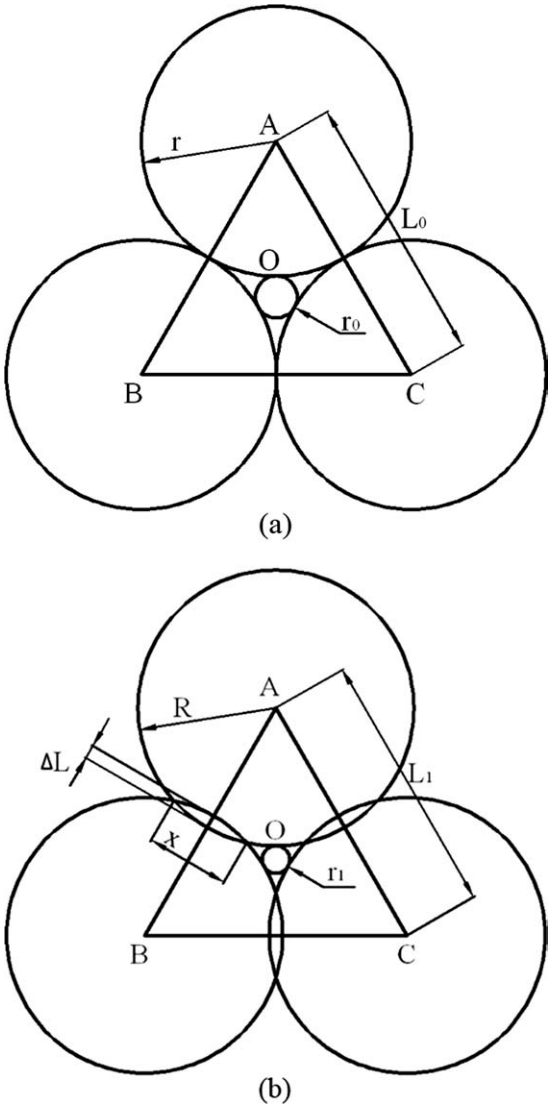

Figure 4 Particle arrangement in UHMWPE microporous materials. (a) Ideal condition; (b) practical condition.

RESULTS AND DISCUSSION

Pore forming mechanism and face-centered cubic structure model

Because polymer particle has a shape of sphere approximately, atomic model of stuffing in crystal structure is applied in this study. In all cumulate

TABLE II
Comparison Between the Calculated Pore Diameter and Actual Data

Group	Particle diameter (μm)	Calculated diameter (μm)	Actual diameter (μm)	Agree or not
R4	300–355	46.50–55.03	52.696	Agree
R5	250–300	38.75–46.50	40.865	Agree
R6	150–180	23.25–27.90	25.957	Agree
R7	80–106	12.40–16.43	14.295	Agree

TABLE III
The Pore Diameter Testing Data of all the Five Samples in Each Group

	Sample 1 (μm)	Sample 2 (μm)	Sample 3 (μm)	Sample 4 (μm)	Sample 5 (μm)	Average	STDEV
Group R4	51.988	52.936	52.807	53.003	52.746	52.696	0.4086
Group R5	41.143	41.547	40.037	40.715	40.883	40.865	0.5592
Group R6	25.775	26.204	26.373	25.918	25.515	25.957	0.3406
Group R7	14.002	14.321	14.596	14.464	14.092	14.295	0.2484
Group R8	52.623	52.371	51.473	51.973	51.635	52.015	0.4838
Group R9	46.011	46.537	46.406	46.815	46.846	46.523	0.3412

textures, face-centered cubic structure is a kind of closest-packed structure,[23,24] which could be used in polymer particles' packing structure to represent the arrangement of the particles. Figure 3 shows the face-centered cubic structure with coordination number 12. Polymer particles are seen as atoms, which position at the six corners of regular hexahedron and center of the six faces. In Figure 3, each numbered particle on the left corresponds to the location in the regular hexahedron on the right. Along the body diagonal, each particle contacts six ones on the same layer and contacts three ones on the adjacent layer. Meanwhile, particles in the same layer cover the same kind of gaps from adjacent layer of particles. When the mold is shocked, polymer particles move within a certain space freely to pack more tightly. Finally, face-centered cubic structure is formed. Here, the packing structure of polymer particles is not a perfect face-centered cubic, because polymer particles' size is not uniform, and the particles are not in the strict sense of a sphere.

When the molding temperature is up to glass transition temperature, UHMWPE macromolecular chain begins to curl and extend partially because of the inside spin of chain segment. Thus, UHMWPE particles get softened from surface to core, and the softened particles move and make packing tightly, which is helpful to establish face-centered cubic packing structure. Because of the continuously heating, the surface of UHMWPE particles is changed into viscous flow state, and the molecular chain segment moves easily, which results that UHMWPE particles join together on the contact surface with chain segments spreading into each other. Then, the heating is stopped, and the mold is cooled down to the room temperature by intermittent water rapidly. The space among the particles after cooling is the reason of pore forming.

The particle arrangement in UHMWPE microporous materials is shown in Figure 4. Under ideal condition, connection between particles is point connection. The pore diameter of microporous materials is just the sphere diameter among three particles, and the sphere is tangent to all three particles, as shown in Figure 4(a). Connecting point *A*, *B*, and *C*, a regular triangle *ABC* was obtained with center of gravity *O*. Pore radius can be calculated under ideal condition by eq. (1):

$$r_0 = 0.155r \tag{1}$$

where r_0 is the pore radius and r is the original particle radius.

However, actually, when the surface of UHMWPE particles is melted, the point connection between particles becomes surface connection, and the interval between particles decreases, as shown in Figure 4(b). Pore radius can be calculated via eq. (2):

$$r_1 = \frac{\sqrt{3}}{3}\left(2r - \frac{x^2}{2R}\right) - R \tag{2}$$

where r_1 is pore radius in practice, r is particle radius before sintering, R is particle radius after sintering, and x is the diameter of contact surface between particles. Considering that the variation of particle radius after sintering is much smaller than original radius and x was much smaller than R, which is ignorable, pore radius could be approximately calculated by eq. (1).

The measured pore diameter and the calculations by the present model for group R4–R7 are shown in Table II. It can be seen from Table II that the experimental measured pore diameter is very close to the

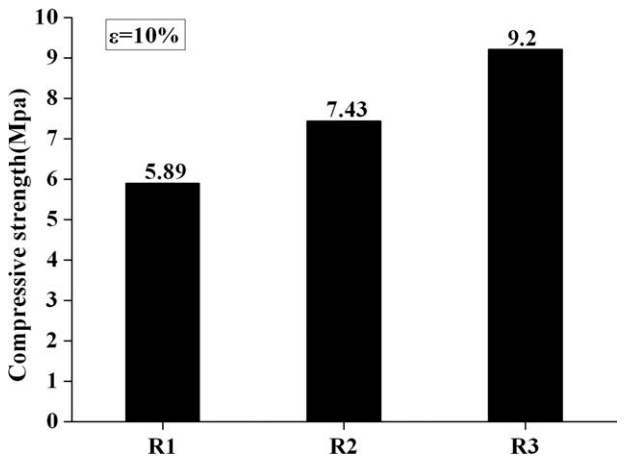

Figure 5 Effect of molecular weight on compressive strength of UHMWPE microporous materials.

TABLE IV
The Compressive Strength Testing Data of All the Five Samples in Each Group

	Sample 1 (MPa)	Sample 2 (MPa)	Sample 3 (MPa)	Sample 4 (MPa)	Sample 5 (MPa)	Average (MPa)	STDEV
Group R1	5.85	5.82	5.90	5.95	5.93	5.89	0.049
Group R2	7.42	7.48	7.45	7.40	7.40	7.43	0.031
Group R3	9.22	9.15	9.24	9.20	9.19	9.20	0.030
Group R4	5.05	5.02	4.97	4.93	4.98	4.99	0.046
Group R5	6.25	6.37	6.29	6.33	6.26	6.30	0.050
Group R6	7.82	7.87	7.91	7.93	7.92	7.89	0.045
Group R7	11.59	11.60	11.64	11.55	11.62	11.60	0.034
Group R8	5.09	5.11	5.00	5.08	5.02	5.06	0.047
Group R9	6.41	6.49	6.44	6.50	6.51	6.47	0.043

range of the value calculated by the model, which indicates the reasonableness and correction of the model. Thus, with the model, pore diameter can be predicted and designed to desirable size. It should be emphasized that eq. (2) can only be used where polymer particle size is not very small.

Here, the actual pore diameter is average pore diameter of five samples in each group. The original testing data of all the five samples in each group are shown in Table III. Every sample in a group was prepared under the same processing conditions. From Table III, it can be seen that STDEV are small, and so average could be more persuasive.

Effect of molecular weight and particle diameter on the performance of microporous materials

Compressive strength is an important parameter in the characterization of microporous materials' performances. We studied the effect of molecular weight on compressive strength of UHMWPE microporous materials, shown in Figure 5. Here, compressive strength is an average of each group. The original testing data of all the five samples in each group are shown in Table IV.

It can be seen from Figure 5 that compressive strength of the samples increases with molecular weight. The reason is due to a longer molecular chain accompanying higher van der Waals forces between molecules. Hence, it helps the enhancement of coherence strength of the samples. Moreover, melt viscosity and adhesive strength between particles are enhanced as molecular weight increases, which results in high-compressive strength.

To study the effect of particle diameter on microporous materials' performance, samples were prepared with same process parameters except for particle diameter, and the results are shown in Table V.

It can be seen from Table V that average pore diameter and porosity both increase with the enhancement of UHMWPE particle diameter while compressive strength and bulk density decrease. In the process of sintering, the heat is conducted from particle surface to core. The bigger the particle size is, the more time it will be needed to melt particle completely, which is advantageous to form big pore. Furthermore, according to FCC structure, pore size increases with particle size. Another important reason for high porosity and big pore size is that for a certain space, it becomes more difficult to form FCC structure as particle size increases. Particles' packing density also decreases as particle size increases. Thus, average pore diameter and porosity of microporous materials increase. Regarding compressive strength, the bigger the particle is, the lower the packing density is, and so the total area of contact surface between particles decreases and coherence strength of materials is lower, which results in the decrease of compressive strength.

Here, porosity and bulk density were measured by weight. The original testing data of all the five samples in each group are shown in Tables VI and VII. From Tables VI and VII, it can be seen that testing data of samples in the same group are consistent, and STDEV are in a small level.

Figure 6 shows the SEM graphs of cross section of UHMWPE microporous materials prepared with different particle diameters. On one hand, it can be seen that UHMWPE particles of the samples are not entirely melted. They pile up together intensively and join at contact surface. The space among particles is the reason of pore forming. Therefore, the SEM graphs verify that face-centered cubic structure of particles' packing exists indeed, and the pore model established before is reasonable. On the other hand, it can also be found from Figure 6 that the

TABLE V
Effect of Particle Diameter on Microporous Materials' Performance

Group	Average pore diameter (μm)	Porosity (%)	Compressive strength (MPa)	Bulk density (g cm^{-3})
R4	52.696	33.9	4.99	0.51
R5	40.865	28.6	6.30	0.59
R6	25.957	26.2	7.89	0.64
R7	14.295	25.3	11.60	0.68

TABLE VI
Porosity Testing Data of All the Five Samples in Each Group

	Sample 1 (%)	Sample 2 (%)	Sample 3 (%)	Sample 4 (%)	Sample 5 (%)	Average (%)	STDEV
Group R4	34.5	33.1	34.4	33.2	34.1	33.9	0.67
Group R5	29.0	28.5	28.2	28.1	29.1	28.6	0.46
Group R6	26.2	26.1	26.1	26.4	26.1	26.2	0.13
Group R7	25.0	25.3	25.1	25.6	25.3	25.3	0.23
Group R8	31.2	32.8	31.9	31.6	32.6	32.0	0.67
Group R9	24.1	24.6	23.8	24.2	24.7	24.3	0.37

space among the particles decreases with the decreasing of UHMWPE particle diameter, which results in small pore size. However, as particle diameter decreases, it is much easier to melt polymer particles excessively, which result that the space among particles is filled partially with the redundant melt, just as shown in Figure 6(d).

For better clarity, Figure 7 shows pore diameter distribution curve based on the data obtained from mercury intrusion porosimeter.

In Figure 7, there is a peaking value of pore size in each curve, which means that there are most pores with this size in volume. It can be found from Figure 7 that pore diameter distribution width of the samples decreases at smaller particle diameter. It appears from the curves that the peaks are narrower too. In Figure 7(a), the peak is centered at about 45 μm and starts flattening at 30–60 μm (±33%). In Figure 7(b), the peak is centered at about 40 μm and starts flattening at 30–50 μm (±33%). In Figure 7(c), the peak is centered at about 25 μm and starts flattening at 15–35 μm (±33%). In Figure 7(d), the peak is centered at about 12 μm and starts flattening at 8–16 μm (±33%). All of which result in concentration of the pore diameter distribution and decreased peaking value of pore size. Thus, it can be concluded that filtration accuracy increases as particle diameter decreases.

Effect of sintering temperature and time on microporous materials' performance

To study the effect of sintering temperature and sintering time on microporous materials' performance, the groups R4 and R8 were prepared at different sintering temperature, and groups R4 and R9 were prepared with different sintering time. The detailed experimental conditions are listed in Table I, and the results are shown in Figure 8.

Compared to R4 at lower sintering temperature, the porosity of R8 is smaller. The same tendency can also be found for sintering time when comparing R4 with R9. Increasing sintering temperature and sintering time both supply more heat to the polymer particles. The more heat transferred to the materials, the more particle surface will be melted in quantity, which results in higher adhesive strength and compressive strength. However, the increase of melting helps the space between particles to be filled with the redundant melt partially, which results in the decreasing of porosity. So, it can be speculated that the space among particles will be fully filled with the melt, and there are no pores if sintering temperature and sintering time are high enough, which is proved by the following SEM graphs in Figure 10.

The pore diameter distribution curve of samples from group R8 and R9 is shown in Figure 9. Comparing Figure 8(a) with Figure 9, it can be seen that as sintering temperature and sintering time increase, pore diameter distribution width increases while peaking value of pore size decreases. Thus, it is safe to conclude that the redundant heat transferred to the materials induces worse uniformity of pore diameter distribution and brings smaller average pore diameter. It should be noted that the available processing temperature range to UHMWPE for sintering is very narrow, and so sintering time has a more important effect on microporous materials' performance than sintering temperature.

Figure 10 shows the SEM graphs of cross section for samples of R8 and R9 with different magnifications.

TABLE VII
Bulk Density Testing Data of All the Five Samples in Each Group

	Sample 1 (g cm^{-3})	Sample 2 (g cm^{-3})	Sample 3 (g cm^{-3})	Sample 4 (g cm^{-3})	Sample 5 (g cm^{-3})	Average	STDEV
Group R4	0.613	0.623	0.614	0.625	0.617	0.618	0.0056
Group R5	0.665	0.669	0.673	0.672	0.663	0.668	0.0042
Group R6	0.691	0.692	0.691	0.689	0.692	0.691	0.0012
Group R7	0.702	0.699	0.701	0.696	0.699	0.700	0.0021
Group R8	0.644	0.629	0.637	0.640	0.631	0.636	0.0062
Group R9	0.711	0.706	0.713	0.709	0.705	0.709	0.0034

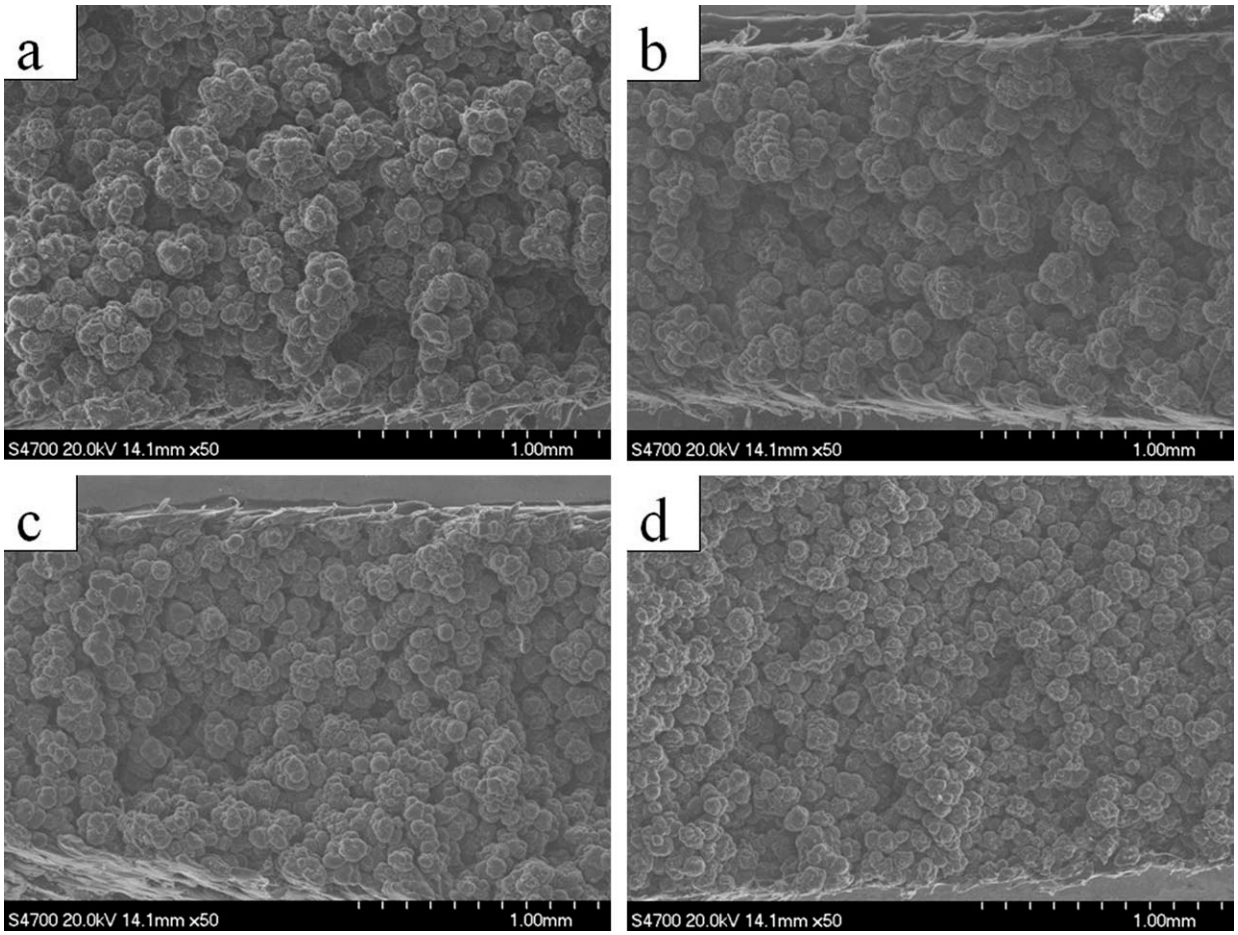

Figure 6 SEM graphs of the cross section of UHMWPE microporous materials. (a) Sample from group R4; (b) sample from group R5; (c) sample from group R6; (d) sample from group R7.

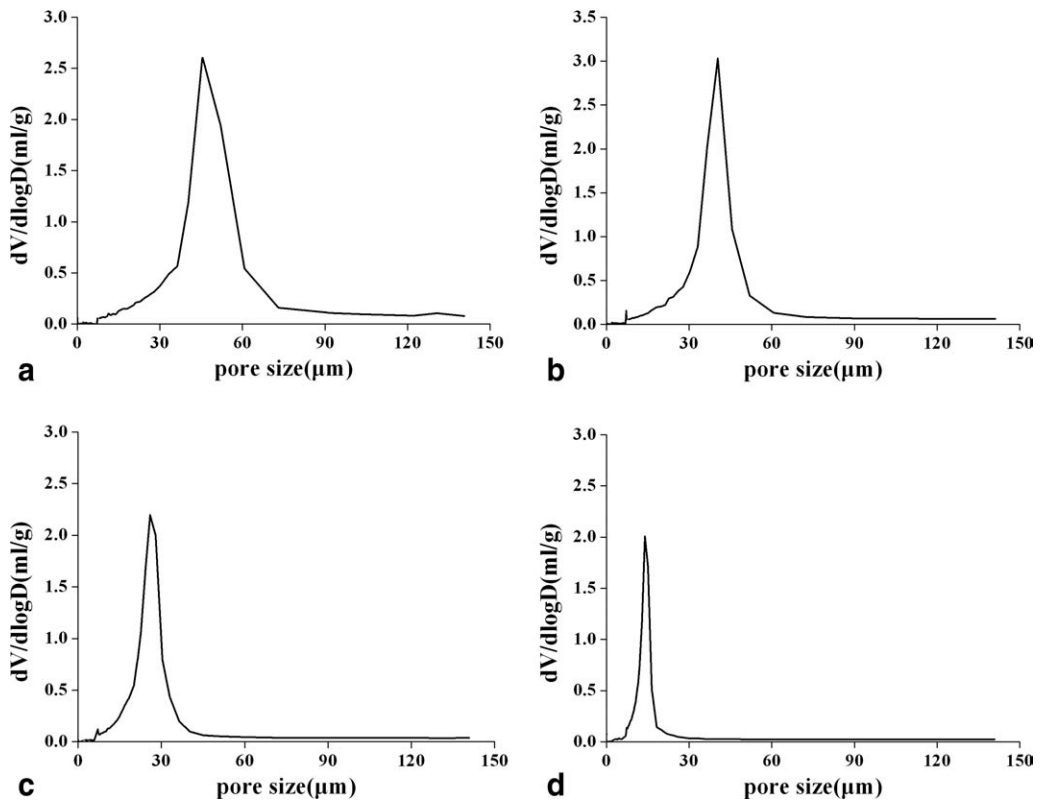

Figure 7 Pore diameter distribution curves of samples prepared with different particle diameter. (a) Sample from group R4; (b) sample from group R5; (c) sample from group R6; (d) sample from group R7.

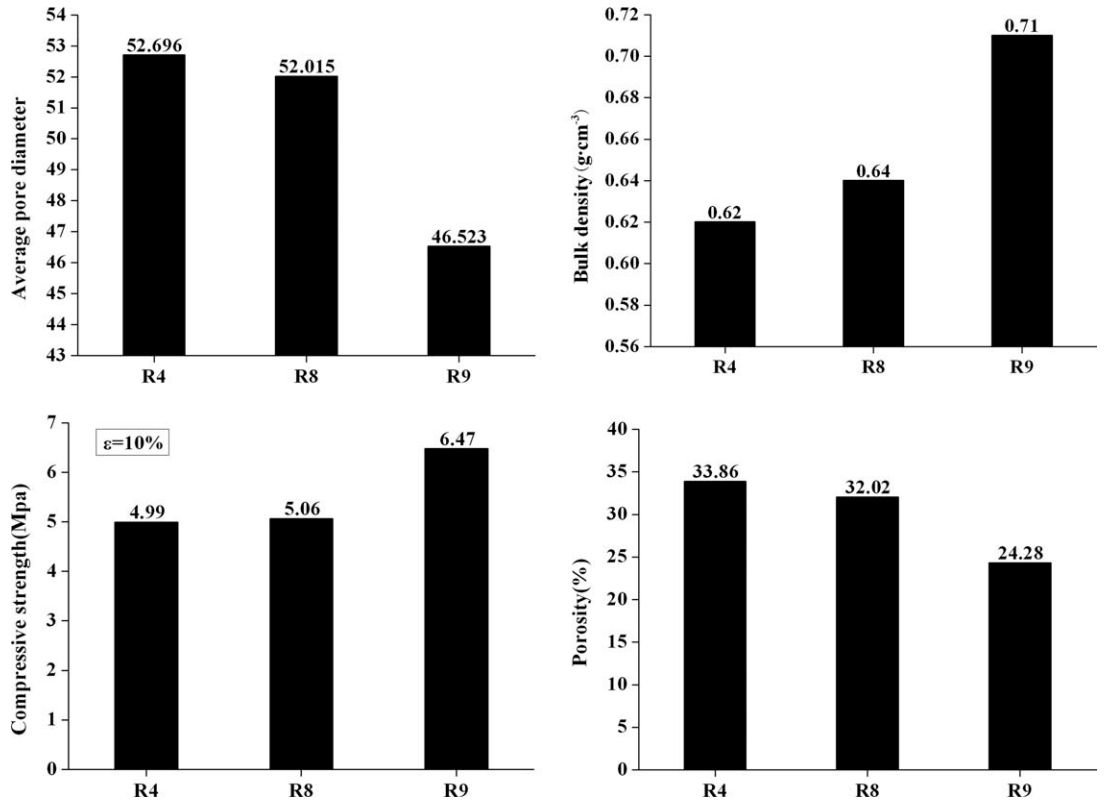

Figure 8 Effect of sintering temperature and sintering time on microporous materials' performance.

Comparing Figure 10 with Figure 6(a), it is seen that as sintering temperature and sintering time increase, more space among the particles is filled with redundant melt, and even the particles melt into a whole solid, as shown in Figure 10(a1,b1), which indicates that redundant heat is not helpful to prepare microporous materials by loose sintering, and there is an optimal processing condition to get desirable pore size.

It should be noted that potential thermal gradients in a large sample during the sintering process need considering. According to thermal gradients, processing conditions can be adjusted. For example, to obtain high-quality sintering sample considering thermal gradients, we can reduce the sintering temperature and extend the sintering time. The research on thermal gradients in large sample with big thickness will be done later.

To prove the reliability of data about samples' performance in this study, some statistical works were done with the data. T-distribution was adopted in the work due to small sample size, and confidence

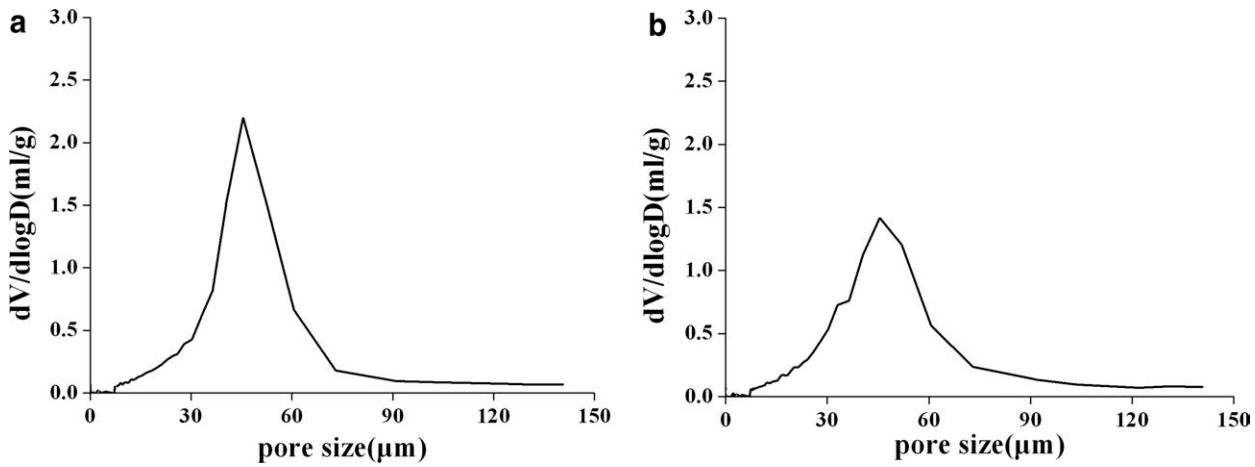

Figure 9 Pore diameter distribution curves of samples from group R8 and R9. (a) Sample from group R8; (b) sample from group R9.

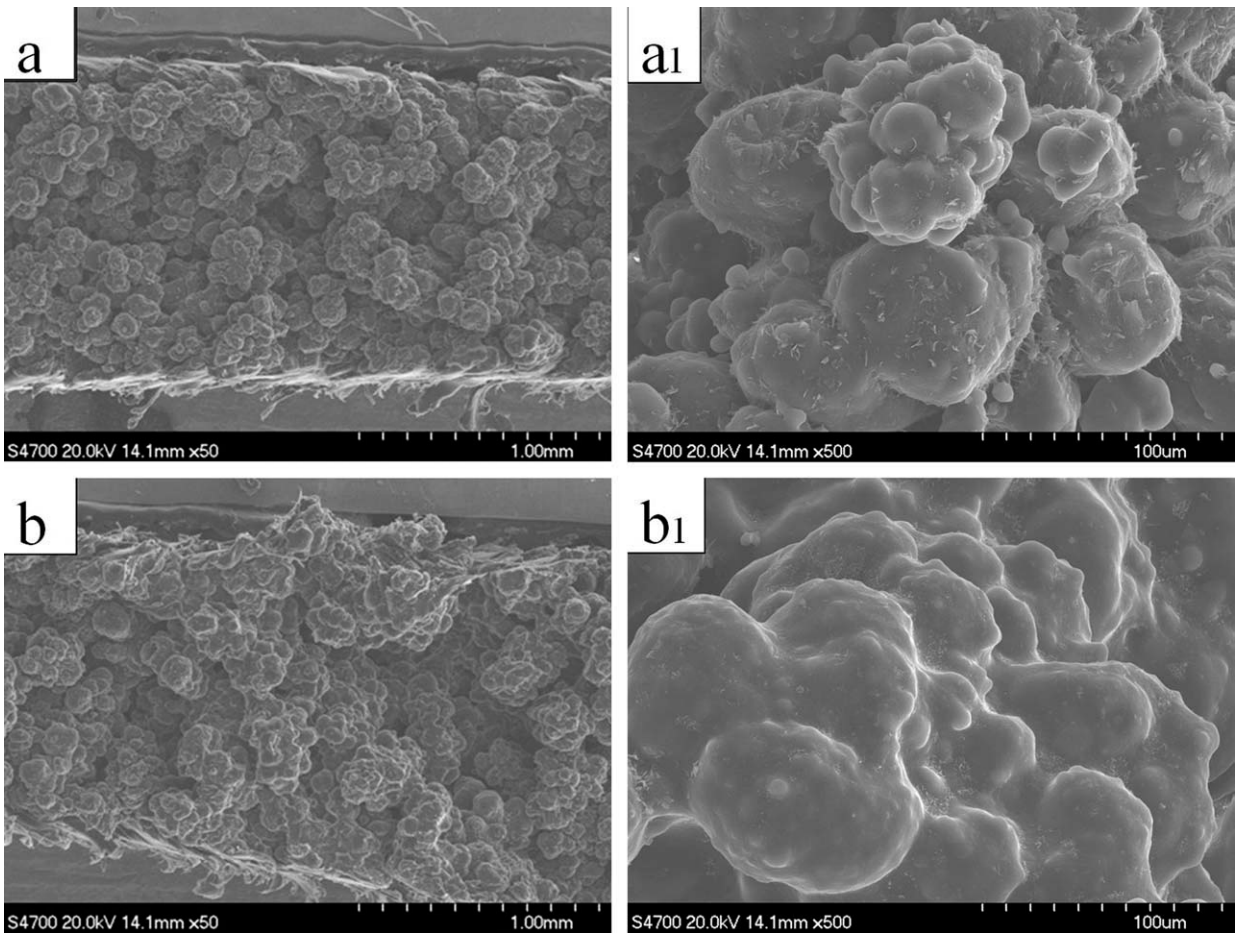

Figure 10 The SEM graphs of the cross section of samples from group R8 and R9. (a) Sample from group R8 magnifying 50; (b) sample from group R9 magnifying 50; (a1) sample from group R8 magnifying 500; (b1) sample from group R9 magnifying 500.

intervals for 95% are shown in Table VIII. We can see from Table VIII that intervals are all narrow enough, and the data concentrate with good reproducibility.

Investigation on uniformity of pore distribution by Fractal Geometry

In 1990, Neimark[25,26] established fractal model as called Neimark model and proposed a method to calculate surface fractal dimension D, which could express the uniformity of pore distribution. In this study, fractal geometry was used to investigate the morphology of UHMWPE microporous materials, and Neimark's model was adopted. The energy conservation can be obtained by the necessary external work of mercury penetrating,[27] as shown in the following:

$$S = -\frac{1}{\gamma\cos\theta}\int_0^{V_P} PdV \tag{3}$$

where γ is the surface tension of mercury (0.458 N/m), θ is the contact angle between the mercury and the

TABLE VIII
Confidence Intervals for 95% on the Data of Samples' Performance (t-Distribution)

Group	Average pore diameter (μm)	Porosity (%)	Compressive strength (MPa)	Bulk density (g cm^{-3})
R1	–	–	5.89 ± 0.061	–
R2	–	–	7.43 ± 0.038	–
R3	–	–	9.20 ± 0.037	–
R4	2.696 ± 0.507	33.9 ± 0.832	4.99 ± 0.057	0.618 ± 0.007
R5	40.865 ± 0.694	28.6 ± 0.571	6.30 ± 0.062	0.668 ± 0.005
R6	25.957 ± 0.423	26.2 ± 0.161	7.89 ± 0.056	0.691 ± 0.001
R7	14.295 ± 0.308	25.3 ± 0.286	11.6 ± 0.042	0.700 ± 0.003
R8	52.015 ± 0.601	32.0 ± 0.832	5.06 ± 0.058	0.636 ± 0.008
R9	46.523 ± 0.424	24.3 ± 0.459	6.47 ± 0.053	0.709 ± 0.004

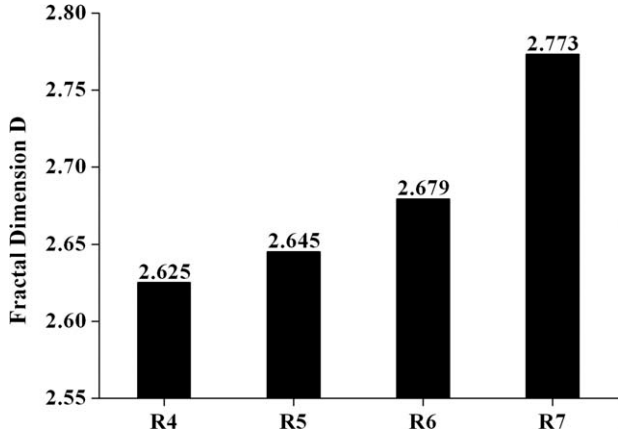

Figure 11 Comparison of fractal dimension D values of samples from different groups.

pore surface (130°); S and V stand for the pore surface and intruded mercury volume, respectively. In this model, the pore is assumed as cylindrical tubes with different radius. To simplify the calculation, the following equation was assumed by Pfeifer and Avnir.[28]

$$\frac{dV}{dr} \propto r^{2-D} \tag{4}$$

where r stands for the pore radius and D is surface fractal dimension with $2 = D = 3$. The mercury intrusion pressure P and the smallest pore size r can be linked by Laplace equation, and the relation is shown in eq. (5):

$$P = \frac{2\gamma\cos\theta}{r} \tag{5}$$

Insert eqs. (4) and (5) into eq. (3) and give the logarithm proportionality, eq. (3) can be simplified as[29]:

$$\log(S) \propto (D-2)\log(P) \tag{6}$$

Linear regression can be made on eq.(6) on the basis of the values of mercury intrusion pressure P and pore surface S supplied by mercury intrusion porosimeter. The gradient of the regression curve is equaled to $(D - 2)$. Thereby, surface fractal dimension D of samples could be obtained easily through eq. (6), and the results are shown in Figure 11.

It can be seen from Figure 11(a) that as particle diameter decreases, fractal dimension value also increases, which means the uniformity of pore distribution becomes worse. From Figure 11(b), it can be found that increasing sintering temperature and sintering time can both lead to high value of D, which corresponds to worse uniformity. The reason is that the redundant heat transferred to the materials can impact pore size, shape, and location and greatly influence uniformity of pore distribution, which also can be confirmed by the analysis of SEM graphs in Figure 10.

CONCLUSIONS

UHMWPE microporous materials were successfully prepared by the new method of loose sintering, and the face-centered cubic structure model was first proposed to calculate the pore size. The results show that the experimental-measured pore diameter is in a good agreement with the value calculated by the present model. Compressive strength of the samples increases with high-molecular weight due to the increasing length of molecular chain. Average pore diameter and porosity both increase with the enhancement of UHMWPE particle diameter while compressive strength and bulk density decrease. Decreasing of particle diameter is helpful to obtain UHMWPE microporous materials with good performance. The porosity decreases and compressive strength increases with the enhancement of sintering temperature or sintering time, because redundant heat can induce small average pore diameter and worse uniformity of pore diameter.

References

1. Turell, M. B.; Bellare, A. Biomaterials 2004, 25, 3389.
2. Harvey, L. S. Engineered Materials Handbook, Vol. 2; ASM International: Materials Park, Ohio, 1999.
3. Goethel, H.; Oberhausen-Sterkrade; Jacob, E.; Oberhausen-Holten; Kolling H.; Hamborn, D.; Roelen, O. U.S. Pat. 3,024,208 (1962).
4. Field, E.; Feller, M.; Forest, P. U.S. Pat. 2,773,053 (1956).
5. Zletz, A.; Forest, P. U.S. Pat. 2,780,617 (1957).
6. Castro, A. J. U.S. Pat. 4,247,498 (1981).
7. Lopatin, G.; Yen, L. Y. U.S. Pat. 4,778,601 (1988).
8. Lopatin, G.; Yen, L. Y. Eur. Pat. 19,799,5A1 (1986).
9. Ding, H. Y.; Tian, Y.; Wang, L. H. J Appl Polym Sci 2007, 105, 3355.
10. Mrozinski, J. S. Eur. Pat. 365,112 (1990).
11. Miller. E. H.; Yaritz, J. G.; Demeuse, M. T.; Whear, J. K. U.S. Pat. 7,682,536 (2010).
12. Inagaki, D.; Kondo, T. U.S. Pat. 7,700,025 (2010).
13. Li, N.; Xiao, C.; Mei, S.; Zhang, S. Desalination 2011, 274, 284.
14. Funaoka, H.; Takita, K.; Kaimai, N.; Kobayashi, S.; Kono, K. U.S. Pat. 7,479,243 (2009).
15. Pluyter, P. B.; Smith, P.; Van Unen, L. H. T.; Rutten, H. J. J. U.S. Pat. 5,248,461 (1993).
16. Pluyter, P. B.; Smith, P.; Van Unen, L. H. T.; Rutten, H. J. J. U.S. Pat. 5,643,511 (1997).
17. Fortuin, H. M.; Simmelink, J. A. P. M. U.S. Pat. 5,370,889 (1994).
18. Fortuin, H. M.; Simmelink, J. A. P. M. U.S. Pat. 5,507,993 (1996).
19. Plumlee, K.; Schwartz, C. J. J Appl Polym Sci 2009, 114, 2555.
20. Li, N.; Xiao, C. J Appl Polym Sci 2011, 117, 2817.
21. Kim, J. J.; Hwang, J. R.; Kim, U. Y. J Membr Sci 1995, 108, 25.
22. Mandelbort, B. B. The Fractal Geometry of Nature. Freeman: San Francisco, 1977.
23. Verhoeven, J. D. Fundamentals of Physical Metallurgy; Wiley: New York, 1975.
24. Guy, A. G.; Hren, J. J. Elements of Physical Metallurgy, 3rd ed.; Addison-Wesley: Reading, MA, 1974.
25. Neimark, A. V. Adsorp Sci Technol 1990, 7, 210.
26. Neimark, A. V. Phys A 1992, 191, 258.
27. Rootare, H. M.; Prenzlow, C. F. J Phys Chem 1967, 71, 2736.
28. Pfeifer, P.; Avnir, D. J Chem Phys 1983, 79, 3558.
29. Friesen, W. I.; Mikula, R. J. Colloid Interf Sci 1987, 120, 263.